eNeuro

Research Article: New Research | Disorders of the Nervous System

Parvalbumin interneuron dysfunction in a thalamo-prefrontal cortical circuit in *Disc1* locus impairment mice

https://doi.org/10.1523/ENEURO.0496-19.2020

Cite as: eNeuro 2020; 10.1523/ENEURO.0496-19.2020

Received: 26 November 2019
Revised: 22 January 2020
Accepted: 27 January 2020

Parvalbumin interneuron dysfunction in a thalamo-prefrontal cortical circuit in *Disc1* locus impairment mice

(Running title: **Parvalbumin interneuron dysfunction in *Disc1* LI mice**)

Kristen Delevich[1,2#], Hanna Jaaro-Peled[4], Mario Penzo[3], Akira Sawa[4], and Bo Li[1,2]

1. Cold Spring Harbor Laboratory, Cold Spring Harbor, NY 11724
2. Watson School of Biological Sciences, Cold Spring Harbor Laboratory, Cold Spring Harbor, NY 11724
3. National Institute of Mental Health, Bethesda, MD, USA 20892
4. Department of Psychiatry, Johns Hopkins University School of Medicine, Baltimore, MD 21287

Author contributions: KD & BL designed research and wrote the paper. KD & MP performed research and KD analyzed data. HJ and AS contributed unpublished reagents and provided feedback on the manuscript.

Corresponding author:

Kristen Delevich, Ph.D.
16 Barker Hall
University of California, Berkeley
Berkeley, California 94720
delevich@berkeley.edu

Keywords: *Disrupted-in-schizophrenia-1*, feedforward inhibition, mediodorsal thalamus, parvalbumin interneurons, prefrontal cortex

5 figures
1 table
0 multimedia
Abstract: 165 words
Significance statement: 112 words
Introduction: 724 words
Discussion: 1464 words

Acknowledgements: We thank members of the B.L. laboratory for discussions.

Conflict of Interest: The authors declare no competing financial interests.

Funding Sources: This work was supported by a National Institutes of Health (NIH) training grant (K.D.), and grants from the NIH (R01MH101214, R01MH108924, B.L.; R01MH094268, R01MH105660, A.S.), National Alliance for Research on Schizophrenia and Depression (NARSAD) (B.L.), the Wodecroft Foundation (B.L.), the Stanley Family Foundation (B.L.), Simons Foundation Autism Research Initiative (SFARI) (B.L.), Louis Feil Trust (B.L.) and the Cold Spring Harbor Laboratory (CSHL) and Northwell Health Affiliation (B.L.).

ABSTRACT

Altered cortical excitation-inhibition (E-I) balance resulting from abnormal parvalbumin interneuron (PV IN) function is a proposed pathophysiological mechanism of schizophrenia (SZ) and other major psychiatric disorders. Preclinical studies have indicated that *disrupted-in-schizophrenia-1* (DISC1) is a useful molecular lead to address the biology of prefrontal cortex dependent cognition and PV IN function. To date, prefrontal cortical inhibitory circuit function has not been investigated in depth in *Disc1* locus impairment (LI) mouse models. Therefore, we used a *Disc1* LI mouse model to investigate E-I balance in medial prefrontal cortical (mPFC) circuits. We found that inhibition onto layer 3 excitatory pyramidal neurons in the mPFC was significantly reduced in *Disc1* LI mice. This reduced inhibition was accompanied by decreased GABA release from local PV, but not somatostatin (SOM) interneurons, and by impaired feedforward inhibition in the mediodorsal thalamus (MD) to mPFC circuit. Our mechanistic findings of abnormal PV IN function in a *Disc1* LI model provide insight into biology that may be relevant to neuropsychiatric disorders including schizophrenia.

SIGNIFICANCE STATEMENT:

A popular theory suggests that dysregulation of fast-spiking parvalbumin interneurons (PV INs) and elevated excitation-inhibition (E-I) balance contribute to the pathophysiology of various psychiatric disorders. Previous studies suggest that genetic perturbations of the *disrupted-in-schizophrenia-1* (*Disc1*) gene affect prefrontal cortex-dependent cognition and PV IN function, but synaptic and circuit physiology data are lacking. Here, we provide evidence that the presynaptic function of PV INs in the medial prefrontal cortex is altered in *Disc1* LI mice and that E-I balance is elevated within a thalamofrontal circuit known to be important for cognition. These findings may contribute to our understanding of the biology that gives rise to cognitive symptoms in a range of neuropsychiatric disorders.

INTRODUCTION

PV INs provide powerful somatic inhibition to excitatory pyramidal neurons and regulate E-I balance (Isaacson and Scanziani, 2011). Prefrontal PV INs are implicated in working memory (WM) function (Cardin et al., 2009; Fries, 2009; Sohal et al., 2009; Murray et al., 2015; Ferguson and Gao, 2018b) and have emerged from human postmortem studies as a key node of interest in the pathophysiology of schizophrenia (Beasley and Reynolds, 1997; Hashimoto et al., 2003; Lewis et al., 2012). Therefore, dysregulation of E-I balance via altered PV IN function is a potential pathophysiological mechanism of particular relevance to cognitive symptoms of neuropsychiatric diseases, including schizophrenia. Cognitive impairment is seen in first-degree relatives of individuals with a range of major mental illnesses (Cannon et al., 2000; Myles-Worsley and Park, 2002; Snitz et al., 2006), suggesting that these processes are partly heritable and may be better understood through investigation of promising genetic and molecular leads.

A translocation in the gene *disrupted-in-schizophrenia-1* (*Disc1*) was first reported in a Scottish pedigree, as a rare but penetrant genetic risk factor that may account for a wide range of major mental illnesses such as depression and schizophrenia (Millar et al., 2000). This suggests that biological pathway(s) involving the multifunctional hub protein DISC1 contribute to cognitive and behavioral dimensions that are disrupted in neuropsychiatric illnesses (Niwa et al, 2016). While DISC1 is not a common genetic variant associated with schizophrenia in large population samples (Schizophrenia Working Group of the Psychiatric Genomics, 2014), it can serve as a molecular lead to study the biology underlying important constructs/dimensions that are relevant to major mental illness (Niwa et al., 2016). Work in mouse models has revealed the importance of DISC1 in neurodevelopment (Kamiya et al., 2005; Ishizuka et al., 2007; Mao et al., 2009; Niwa et al., 2010; Ishizuka et al., 2011), synaptic function (Hayashi-Takagi et al., 2010; Wang et al., 2011; Maher and LoTurco, 2012; Sauer et al., 2015; Seshadri et al., 2015; Wei et al., 2015), and cognitive processing (Brandon and Sawa, 2011). WM impairments are consistently reported across *Disc1* mouse models (Koike et al., 2006; Clapcote et al., 2007; Li et

al., 2007; Kvajo et al., 2008; Lipina et al., 2010; Niwa et al., 2010; Brandon and Sawa, 2011; Lee et al., 2013). Furthermore, a variety of *Disc1* mouse models exhibit reduced prefrontal PV expression (Hikida et al., 2007; Shen et al., 2008; Ibi et al., 2010; Niwa et al., 2010; Ayhan et al., 2011; Lee et al., 2013). While this data is suggestive that PV INs may be particularly affected by *Disc1* perturbation, evidence from synaptic and circuitry physiology is lacking.

Here, we investigated the synaptic and circuit level function of PV INs within the prefrontal cortex (mPFC) circuits of mice heterozygous for the *Disc1* locus impairment (LI) allele, in which the majority of *Disc1* isoforms are abolished (Seshadri et al., 2015; Shahani et al., 2015). We found that *Disc1* LI was associated with elevated E-I balance and abnormal PV IN function in mPFC circuits relevant to cognition.

MATERIALS AND METHODS

Animals

Mice were group housed under a 12-h light-dark cycle (9 a.m. to 9 p.m. light), with food and water freely available. Both male and female mice were used. All procedures involving animals were approved by the Institute Animal Care and Use Committees of Cold Spring Harbor Laboratory and conducted in accordance to the US National Institute of Health guidelines. The *PV-Cre* (http://jaxmice.jax.org/strain/008069.html), *SOM-Cre* (http://jaxmice.jax.org/strain/013044.html), and *Ai14* (https://www.jax.org/strain/007914) mice were described previously (Hippenmeyer et al., 2005; Madisen et al., 2010; Taniguchi et al., 2011). We previously generated the *Disc1* LI mice, which harbor a deletion (6.9 kb) encompassing the first 3 exons of the *Disc1* gene (Seshadri et al., 2015). The majority of DISC1 isoforms are abolished in mice homozygous for the *Disc1* LI allele (Seshadri et al., 2015), and in the current study we used mice that harbored one *Disc1* LI allele (+/-). All mice have been bred onto C57BL/6 background for at least 5 generations.

Viral vectors

Adeno-associated virus (AAV) vectors AAV-CAG-ChR2(H134R)-YFP and AAV-eF1a-DIO-ChR2(H134R)-YFP were produced as AAV2/9 serotype by the University of North Carolina Vector Core (Chapel Hill, NC) and have been previously described (Zhang et al., 2007; Delevich et al., 2015). All viral vectors were stored in aliquots at –80°C until use.

Stereotaxic surgery

Mice aged postnatal day 40 to 56 (P40-P56) were used for all surgeries. Unilateral viral injections were performed using previously described procedures (Li et al., 2013) at the following stereotaxic coordinates: MD, –1.58 mm from Bregma, 0.44 mm lateral from midline, and 3.20 mm vertical from cortical surface; dorsal mPFC: 1.94 mm from Bregma, 0.34 mm lateral from midline, and 0.70 mm vertical from cortical surface. Surgical procedures were standardized to minimize the variability of AAV injections. To ensure minimal leak into surrounding brain areas, injection pipettes remained in the brain for ~5 min post-injection before being slowly withdrawn. The final volume for AAV-CAG-ChR2(H134R)-YFP injected into MD was 0.3–0.35 μl, and for AAV-eF1a-DIO-ChR2(H134R)-YFP injected into dorsal mPFC was 0.5 μl. The titer for the viruses was ~10^{12} viral particles/ml. For experiments in which mPFC inhibitory interneurons were optogenetically stimulated (Figure 2) mice were injected at P56 and ~2 weeks were allowed for viral expression before recording. For experiments in which MD axons within mPFC were optogenetically stimulated (Figures 3 & 5) mice were injected at P40-45 and ~4 weeks were allowed for viral expression before recording. For each of these experiments, littermates were injected and recorded at the same age to control for expression duration between genotypes.

Electrophysiology

Mice were anaesthetized with isoflurane and decapitated, whereupon brains were quickly removed and immersed in ice-cold dissection buffer (110.0 mM choline chloride, 25.0 mM

105 $NaHCO_3$, 1.25 mM NaH_2PO_4, 2.5 mM KCl, 0.5 mM $CaCl_2$, 7.0 mM $MgCl_2$, 25.0 mM glucose,
106 11.6 mM ascorbic acid and 3.1mM pyruvic acid, gassed with 95% O_2 and 5% CO_2). Coronal
107 slices (300 μm in thickness) containing mPFC were cut in dissection buffer using a HM650
108 Vibrating Microtome (Thermo Fisher Scientific), and were subsequently transferred to a
109 chamber containing artificial cerebrospinal fluid (ACSF) (118 mM NaCl, 2.5 mM KCl, 26.2 mM
110 $NaHCO_3$, 1 mM NaH_2PO_4, 20 mM glucose, 2 mM $MgCl_2$ and 2 mM $CaCl_2$, at 34 °C, pH 7.4,
111 gassed with 95% O_2 and 5% CO_2). After ~30 min recovery time, slices were transferred to room
112 temperature and were constantly perfused with ACSF.

113 The internal solution for voltage-clamp experiments contained 140 mM potassium
114 gluconate, 10 mM HEPES, 2 mM $MgCl_2$, 0.05 mM $CaCl_2$, 4 mM MgATP, 0.4 mM Na_3GTP, 10
115 mM Na_2-Phosphocreatine, 10 mM BAPTA, and 6 mM QX-314 (pH 7.25, 290 mOsm).
116 Electrophysiological data were acquired using pCLAMP 10 software (Molecular Devices).
117 mIPSCs were recorded in the presence of tetrodotoxin (1 μM), APV (100 μM), and CNQX (5
118 μM). mEPSCs were recorded in the presence of tetrodotoxin (1 μM) and picrotoxin (100 μM).
119 Data were analyzed using Mini Analysis Program (Synaptosoft). For the mIPSCs and mEPSCs,
120 we analyzed the first 300 and 250 events, respectively, for each neuron. The parameters for
121 detecting mini events were kept consistent across neurons, and data were quantified blindly
122 with regard to the genotypes.

123 To evoke synaptic transmission by activating ChR2, we used a single-wavelength LED
124 system (λ = 470 nm, CoolLED.com) connected to the epifluorescence port of the Olympus BX51
125 microscope. To restrict the size of the light beam for focal stimulation, a built-in shutter along the
126 light path in the BX51 microscope was used. Light pulses of 0.5-1 ms triggered by a TTL
127 (transistor-transistor logic) signal from the Clampex software (Molecular Devices) were used to
128 evoke synaptic transmission. The light intensity at the sample was ~0.8 mW/mm^2.
129 Electrophysiological data were acquired and analyzed using pCLAMP 10 software (Molecular
130 Devices). IPSCs were recorded at 0 mV holding potential in the presence of 5 μM CNQX and

100 μM AP-5. Light pulses were delivered once every 10 seconds, and a minimum of 30 trials were collected. In paired-pulse recordings, 2 light pulses separated by 50, 100, or 150 ms were delivered. In cases that the first IPSC did not fully decay to baseline before the onset of the second IPSC, the baseline of the second IPSC was corrected before the peak was measured. To measure the kinetics of the IPSCs, averaged sweeps collected at the 150 ms interval were normalized, and the decay time constant and half-width were measured using automated procedures in the AxoGraph X 1.5.4 software.

To determine IPSC reversal potential (E_{IPSC}), IPSCs were recorded at varying holding potentials (20 mV steps) in the presence of CNQX (5 μM) and APV (100 μM) to block AMPA receptors and NMDA receptors, respectively. IPSC amplitude was measured, and a linear regression was used to calculate the best-fit line, and the x-intercept was used as the E_{IPSC}. Under our recording conditions, the E_{IPSC} was ~ –60 mV. Therefore, in the excitation/inhibition ratio (E/I) experiments, we recorded EPSCs at –60 mV and IPSCs at 0 mV holding potential. The only drug used for the E/I experiments was APV (100 μM). In these experiments we used the same light intensity for evoking both IPSCs and EPSCs. In addition, we used similar stimulation regime for WT and *Disc1* LI mice, such that the peak amplitudes of IPSCs are comparable between genotypes.

For the experiments in which we optogenetically stimulated the MD axons in the mPFC, mice were excluded if the extent of infection in the MD was too large and leaked into surrounding brain regions. Rodent MD lacks interneurons; therefore all ChR2 infected neurons are expected to be relay projection neurons (Kuroda et al., 1998).

The latency and 10-90% rise-time of EPSCs and IPSCs were calculated from either the averaged trace or individual sweeps for each cell using automated procedures in the AxoGraph X 1.5.4 software. ESPC and IPSC onset latency was calculated as the time from stimulation onset to 10% rise time, with EPSC-IPSC delay calculated as the difference. The 10% rise time has been reported to be a more reliable measure of delay to onset, as it minimizes the

157 contribution of EPSC and IPSC rise time differences that are reflected in the time to peak
158 (Mittmann et al., 2005). Some of the control data from WT mice used for comparing with *Disc1*
159 LI mice (appearing in Fig. 3, 4) were previously reported in Fig. 1, 2, and 4 of (Delevich et al.,
160 2015).

161 **Data analysis and statistics**

162 All statistical tests were performed using Origin 9.0 (Origin-Lab, Northampton, MA) or
163 GraphPad Prism 6.0 (GraphPad Software, La Jolla, California) software. All data were tested for
164 normality using the D'Agostino-Pearson omnibus normality test to guide the selection of
165 parametric or non-parametric statistical tests. Data are presented as mean ± s.e.m. or median ±
166 interquartile range as indicated. For parametric data, a two-tailed *t* test or two-way ANOVA was
167 used, with a *post hoc* Sidak's test for multiple comparisons. For non-parametric data, a two-
168 tailed Mann-Whitney U test was used. $P < 0.05$ was considered significant. A summary of the
169 statistical analyses performed can be found in Table 1.

170

171 **RESULTS**

172 **Inhibitory synaptic transmission is impaired in adult *Disc1* LI mice**

173 As a first estimation of inhibitory drive in the mPFC, we recorded mIPSCs onto L2/3 PNs
174 in the dorsal anterior cingulate cortex (dACC) subregion of the mPFC in adult mice (postnatal
175 day (P) 70). We found that compared with wild-type (WT) littermates, *Disc1* LI mice had
176 significantly reduced mIPSC frequency (WT, 3.75 ± 3.25 Hz, n = 27 cells, N= 6; *Disc1* LI, 2.27 ±
177 2.72 Hz, n = 29 cells, N=5; $U = 217.0$, $^{a}P < 0.01$, Mann-Whitney U test), but not amplitude (WT,
178 12.5 ± 2.48 pA, n = 29 cells, N= 6; *Disc1* LI, 12.52 ± 1.51 pA, n = 27 cells, N=5; $U = 351.0$, $^{b}P =$
179 0.51, Mann-Whitney U test) (Fig. 1A–C). The two groups did not differ in measures of miniature
180 excitatory postsynaptic currents (mEPSC) (frequency: WT, 3.47 ± 1.97 Hz, n = 23 cells, N=4;
181 *Disc1* LI, 2.79 ± 2.4 Hz, n = 20 cells, N=5; $U = 173.0$, $^{c}P = 0.17$, Mann-Whitney U test;
182 amplitude: WT, 8.91 ± 0.18 pA; *Disc1* LI, 8.99 ± 0.37 pA, $t_{(41)} = 0.18$, $^{d}P = 0.86$, *t*-test) (Fig. 1D–

F). Notably, we found that the frequency (but not amplitude) of mIPSCs recorded from dACC L2/3 PNs in *Disc1* LI mice was lower than their WT littermates at preweanling (~P15) age amplitude (amplitude: WT, n = 44 cells; *Disc1* LI, n = 26 cells; [e]$P = 0.12$, *t* test; frequency: WT, n = 44 cells; *Disc1* LI, n = 26 cells; [f]$P < 0.05$, Mann-Whitney U test) (Fig. 1G-I). These data indicate that the inhibitory synaptic transmission is selectively impaired in the mPFC of *Disc1* LI mice, and that this impairment manifests early in postnatal development.

Altered presynaptic function of PV interneurons in *Disc1* LI mice

A reduction in mIPSC frequency could result from a decrease in synaptic transmission from one or more inhibitory IN populations. To investigate the source of reduced inhibitory drive onto L2/3 PNs in the mPFC of *Disc1* LI mice, we sought to examine the IPSCs originating from either PV or SOM INs. To this end, we selectively expressed channelrhodopsin (ChR2), the light-gated cation channel (Zhang et al., 2006), in PV or SOM INs by injecting the mPFC of *Disc1* LI*; PV-Cre* or *Disc1* LI*; SOM-Cre* mice, as well as their wild-type (WT) littermates, with an adeno-associated virus (AAV) expressing ChR2 in a Cre-dependent manner (AAV-DIO-ChR2(H134R)-YFP). After viral expression had reached sufficient levels, we prepared acute brain slices from these mice and recorded from mPFC L2/3 PNs light-evoked IPSCs (Fig. 2A, D). We used paired light pulses (pulse duration 1 ms) with an inter-pulse-interval of 50, 100, or 150 ms, and measured the ratio of the peak amplitude of the second IPSC over that of the first ($IPSC_2/IPSC_1$), also known as paired-pulse ratio (PPR) (Fig. 2B, E). A similar technique has previously been used to interrogate presynaptic GABA release from PV interneurons (Chu et al., 2012).

We found that the PPR of GABAergic transmission between PV INs and L2/3 PNs was significantly increased in the *Disc1* LI mice compared with their WT littermates at the 50 and 100 ms inter-pulse-intervals (WT, n = 13 cells; *Disc1* LI, n = 10 cells; interval: $F(2, 42) = 6.77$, [g]$P < 0.01$; genotype: $F(1, 21) = 10.77$, $P < 0.01$; interaction: $F(2, 42) = 3.92$, $P < 0.05$; two-way repeated-measures (RM) ANOVA followed by Sidak's tests) (Fig. 2C), suggesting that GABA

release from PV INs is impaired. In contrast, the PPR of GABAergic synaptic transmission from SOM INs to L2/3 PNs did not differ between genotypes (WT, n = 15 cells, *Disc1* LI, n = 12 cells; interval: F(2, 50) = 24.88, [h]*P* < 0.0001; genotype: F(1, 25) = 1.64, *P* = 0.21; interaction F(2, 50) = 0.47, *P* = 0.63, two-way RM ANOVA) (Fig. 2F). SOM-evoked IPSCs displayed significantly slower decay kinetics than PV-evoked IPSCs (Fig. 2G, H), consistent with previous reports (Koyanagi et al., 2010; Ma et al., 2012). No differences in IPSC kinetics were observed between *Disc1* LI mice and their WT littermates (cell type: F(1, 46) = 90.82, [i]*P* < 0.0001; genotype: F(1,46) = 0.678, *P* = 0.41; two-way ANOVA) (Fig. 2G, H). In light of the observed reduction in mIPSC frequency, the increased PPR of PV-mediated IPSCs suggests that there is a presynaptic deficit in GABA release from PV cells to L2/3 PNs in the mPFC of *Disc1* LI mice.

Reduced feedforward inhibition in a thalamus–mPFC circuit in *Disc1* LI mice

The mediodorsal nucleus of the thalamus (MD) sends major projections to the mPFC. This MD–mPFC circuit has been implicated in cognitive processes such as working memory (Parnaudeau et al., 2013; Bolkan et al., 2017; Parnaudeau et al., 2017; Ferguson and Gao, 2018b) and cognitive flexibility (Parnaudeau et al., 2015; Rikhye et al., 2018) that are impaired in schizophrenia (Lesh et al., 2011; Parnaudeau et al., 2013; Parnaudeau et al., 2015). We and others have shown that excitatory inputs from the MD drive mPFC feedforward inhibition (FFI) (Miller et al., 2017; Collins et al., 2018; Meda et al., 2019) that is primarily mediated by mPFC PV INs (Delevich et al., 2015). Given the deficit in GABA release from PV INs to PNs in the mPFC of *Disc1* LI mice (Fig. 2), we reasoned that FFI in the MD–mPFC circuit is affected in these mice. To test this hypothesis, we injected the MD of *Disc1* LI mice and their WT littermates with AAV-ChR2(H134R)-YFP. After viral expression reached sufficient levels we used these mice to prepare acute brain slices, in which we recorded both excitatory and inhibitory synaptic transmission onto dACC L3 PNs in response to optogenetic stimulation of MD axons (Fig. 3A, B).

Brief (0.5 ms) light stimulation evoked monosynaptic EPSCs and disynaptic IPSCs in L3 PNs in the dorsal mPFC (Fig. 3C) (and see (Delevich et al., 2015)). We found that the contribution of inhibitory synaptic transmission to total synaptic inputs – measured as $IPSC^{peak}/(IPSC^{peak}+EPSC^{peak})$, or $I^{peak}/(I^{peak}+E^{peak})$ – was significantly lower in *Disc1* LI mice than in WT mice when comparing the means of the two groups of animals (*Disc1* LI, 0.52 ± 0.03, N = 11 mice; WT, 0.70 ± 0.02, N = 14 mice; $t_{(23)} = 5.73$, $^{j}P < 0.0001$, *t* test) (Fig. 3 D), or the means of the two groups of neurons (*Disc1* LI, 0.60 ± 0.03; n = 30 cells, WT, 0.70 ± 0.02, n = 40 cells; $t_{(68)} = 3.17$, $^{k}P < 0.01$, *t* test) (Fig. 3 E). In addition, the slope of a linear regression describing the relationship between IPSCs and EPSCs of individual neurons in the *Disc1* LI mice was significantly lower than that in the WT (Fig. 3F). The latencies (Fig. 3G-I) and kinetics of the EPSCs (Fig. 3J-K) and IPSCs (Fig. 3L-M) in *Disc1* LI mice were similar to those in WT mice. These results together indicate that *Disc1* LI is associated with reduced MD-driven FFI in the mPFC.

Spontaneous excitatory synaptic transmission onto PV interneurons and their intrinsic properties are unchanged in *Disc1* LI mice

The decrease in FFI in the MD–mPFC pathway in *Disc1* LI mice could result from the impairment in GABA release from PV INs in the mPFC (Fig. 2), or reduced recruitment of mPFC PV INs by MD. Thalamically-driven feedforward inhibition relies on the ability of PV INs to reach threshold in response to thalamic inputs, a process dependent on both synaptic and intrinsic properties of PV INs. DISC1 is expressed in MGE-derived inhibitory interneurons including PV INs (Schurov et al., 2004; Meyer and Morris, 2008; Steinecke et al., 2012; Seshadri et al., 2015) raising the possibility that *Disc1* LI could alter excitatory synaptic transmission onto PV INs and/or their intrinsic properties. We crossed the *Disc1* LI mouse line onto the *PV-Cre::tdTomato* lines, thereby allowing us to assess the synaptic and intrinsic properties of visually identified PV INs in the context of *Disc1* LI. We found that mEPSC amplitude and frequency onto mPFC PV INs was consistent between genotypes (amplitude: WT, 12.39 ± 0.40 pA; *Disc1* LI, 13.48 ± 0.45

pA, n= 20, 23 cells/genotype, N=4, 4 mice/genotype; $t_{(41)}$= 1.78, [l]P= 0.08; frequency: WT, 6.99 ± 0.74 Hz; *Disc1* LI, 6.55 ± 0.69 Hz, $t_{(41)}$= 0.53, [m]P=0.60) (Fig. 4A-B). Next, we examined the intrinsic properties of PV INs in WT and *Disc1* LI mice and found no significant differences between genotypes (Fig. 4C-H), including minimum current injection required to elicit spiking (WT, 142.3 ± 12.67 pA; *Disc1* LI, 119.2 ± 14.3 pA, $t_{(24)}$= 1.21, [n]P= 0.24) (Fig. 4G) or maximum firing rate (WT, 88.92 ± 3.9 Hz; *Disc1* LI, 88.92 ± 6.78 Hz, $t_{(24)}$ = 0, [o]P > 0.99) (Fig. 4H). These results suggest that neither intrinsic excitability of prefrontal PV INs nor spontaneous glutamatergic transmission onto them is grossly perturbed in *Disc1* LI mice.

Enhanced input but reduced output of PV interneurons in *Disc1* LI mice

We next examined recruitment of mPFC PV INs specifically within the MD–mPFC circuit to determine whether reduced excitatory drive could account for the observed reduction in FFI in *Disc1* LI mice. We recorded evoked EPSCs from PV IN and PN pairs in the mPFC in response to optogenetic stimulation of MD axons (Fig. 5A). We found that in WT mice, amplitudes of thalamocortical EPSCs were similar between PV INs and neighboring PNs (PV, -109.3 ± 109.7 pA, PN, -129.1 ± 103.2 pA, n = 15 pairs, W = 0, [p]P = 1.0, Wilcoxon matched-pairs signed rank test) (Fig. 5B, C). By contrast, in *Disc1* LI mice, thalamocortical EPSCs onto PV INs were much larger than those onto neighboring PNs (PV, -153.4 ± 211.9 pA; PN, -73.74 ± 104.6 pA; n = 14 pairs, W = -83, [q]P < 0.01 Wilcoxon matched-pairs signed rank test) (Fig 5B, C). These data suggest that MD excitatory drive onto PV INs is enhanced relative to L2/3 PNs in the mPFC of *Disc1* LI mice. Therefore, reduced excitatory synaptic strength onto PV INs doesn't account for the decrease in FFI in the MD–mPFC circuit in *Disc1* LI mice compared to WT (Fig. 3).

Next, we probed presynaptic GABA release from PV cells within the MD–mFPC circuit, by optogenetically stimulating the MD axons (see the recording configuration in Fig. 3A & B) and measuring the PPR of MD-driven FFI onto mPFC PNs (Fig. 5D). Notably, we found that PPR of was significantly higher in *Disc1* LI mice than in WT mice (WT: 0.0 ± 0.1, n = 24 cells, N= 10; *Disc1* LI: 0.24 ± 0.34, n = 17 cells, N=6; U = 62, [r]P = 0.0001, two-tailed Mann Whitney U test)

(Fig. 5D, E), mirroring the increase in PPR we observed when directly activating PV INs (Fig. 2C). In order to reduce variability in measuring the PPR, we set the light-stimulation such that there was no difference between genotypes in the average amplitude of the first evoked IPSCs (WT, 439.3 ± 41.31 pA, n = 24 cells, N=10; *Disc1* LI, 367.1 ± 46.26 pA, n = 17 cells, N=6; $t_{(39)}$ = 1.152, ^{s}P = 0.256, unpaired *t* test) (Fig. 5F). Finally, we examined the relationship between PPR of MD-driven FFI and E-I ratio of MD-driven synaptic currents onto PNs. We found that there was a significant inverse correlation between FFI PPR and $I^{peak}/(I^{peak}+E^{peak})$ within PNs from *Disc1* LI mice but not WT mice (Fig. 5G). Together, our data suggest that in *Disc1* LI mice, GABA release from prefrontal PV INs is reduced, leading to decreased FFI in the MD–mPFC circuit.

Discussion

Perturbation of the multifunctional scaffolding protein DISC1 is linked to a range of behavioral phenotypes that are associated with major psychiatric disorders (Brandon and Sawa, 2011). These findings highlight DISC1 as a promising molecular lead to investigate the molecular pathways and neural circuits that underlie major mental illnesses (Niwa et al., 2016). Here, we used the *Disc1* LI mouse model to investigate the function of mPFC circuits that may be particularly relevant to the cognitive symptoms of psychiatric disorders. We found that *Disc1* LI exhibited elevated E-I ratio, measured as a reduction of spontaneous inhibitory transmission onto L2/3 PNs in mPFC and decreased FFI onto L2/3 PNs in the MD–mPFC circuit. Several lines of evidence suggest that this effect can be accounted for by a reduction in GABA release from PV INs in the mPFC 1) mIPSC frequency was significantly reduced onto L2/3 PNs in *Disc1* LI mice, consistent with a reduction in presynaptic release probability; 2) the PPR of IPSCs directly evoked by optogenetic stimulation of PV INs but not SOM INs was significantly increased in *Disc1* LI mice compared to WT; and 3) the PPR of MD-evoked FFI – which is almost exclusively driven by PV INs under the experimental conditions used (Delevich et al., 2015) – was increased in *Disc1* LI mice and correlated with E-I ratio. Together, our findings

suggest that the PV→PN synapses are the primary site of impairment in the MD–mPFC circuit in *Disc1* LI mice.

It has been hypothesized that the cognitive deficits in psychiatric diseases may be the consequence of imbalanced excitation and inhibition (E-I) in key neural circuits (Kehrer et al., 2008; Lisman, 2012; Marin, 2012; Krystal et al., 2017; Ferguson and Gao, 2018a). Consistent with this hypothesis, several studies have shown that experimentally imposing elevated E-I within the mPFC impairs cognitive processing in rodents (Yizhar et al., 2011; Cho et al., 2015; Murray et al., 2015; Ferguson and Gao, 2018b). In addition to evidence of altered PV IN mediated inhibition, we observed that excitatory synaptic transmission onto PV cells driven by MD inputs was enhanced in *Disc1* LI mice, which could compensate for presynaptic deficits in PV IN function. Indeed, a recent study that examined multiple autism genetic mouse models found that increased E-I ratio did not drive network hyperexcitability but in fact led to homeostatic stabilization of excitability (Antoine et al., 2019). Therefore, potential network effects arising from altered E-I conductance ratios should not be over interpreted, and it remains unclear how the changes we observed in the *Disc1* LI mice affect network activity *in vivo* and resulting behavior.

In humans, *Disc1* polymorphisms are associated with measures of cognitive performance and frontal lobe structure among some ethnic groups (Burdick et al., 2005; Cannon et al., 2005; Hennah et al., 2005; Liu et al., 2006; Palo et al., 2007; Carless et al., 2011; Nicodemus et al., 2014). Multiple mouse models of DISC1 perturbation exhibit cognitive impairments (Koike et al., 2006; Clapcote et al., 2007; Li et al., 2007; Kvajo et al., 2008; Lipina et al., 2010; Niwa et al., 2010; Brandon and Sawa, 2011; Lee et al., 2013), strengthening the mechanistic link between DISC1 and cognition. Here we provide evidence of cell type-specific alterations within mPFC circuits implicated in multiples aspects of cognition. While we did not examine cognition in the *Disc1* LI mice, *Disc1* LI (-/-) mice are reported to exhibit blunted startle response and prepulse inhibition (PPI) (Jaaro-Peled et al., 2018), a behavior that is regulated by

338 the mPFC (Swerdlow et al., 2001; Schwabe and Koch, 2004; Jaaro-Peled et al., 2018). Future
339 experiments interrogating mPFC-dependent cognition in *Disc1 LI* mice will be critical for relating
340 the circuit-level changes we observed in E-I balance and PV IN function to behavior.

341 While our study is the first to specifically detect a presynaptic deficit in PV INs in a
342 DISC1 genetic deficiency model, previous studies using different transgenic models have
343 reported that DISC1 influences inhibitory IN function or development: spontaneous IPSC
344 frequency is reduced in the frontal cortex of male mice expressing a truncated mouse DISC1
345 (Holley et al., 2013); PV IN function is impaired in the mPFC of mice overexpressing a truncated
346 form of DISC1 (Sauer et al., 2015); PV expression is reduced in the PFC of several *Disc1*
347 mouse models (Hikida et al., 2007; Shen et al., 2008; Niwa et al., 2010; Ayhan et al., 2011; Lee
348 et al., 2013); and tangential migration of MGE-derived neurons is impaired by *Disc1* mutation or
349 RNA interference (Steinecke et al., 2012; Lee et al., 2013). These findings provide converging
350 evidence that DISC1 perturbation alters prefrontal cortical inhibition. Our current findings more
351 specifically implicate the presynapse of PV INs as a site of impairment in mice harboring a
352 *Disc1* LI allele, which is the most extensively perturbed form of the gene reported to date
353 (Shahani et al., 2015).

354 Several important caveats should be considered when interpreting our electrophysiology
355 results. First, a reduction in mIPSC frequency is also consistent with a reduced number of
356 inhibitory synapses. However, a recent study investigating *Disc1* LI mice reported no change in
357 the number of PV INs themselves within the mPFC (Seshadri et al., 2015). In addition, we
358 focused on PV and SOM IN function, which together comprise ~70% of cortical INs (Rudy et al.,
359 2011). It is therefore possible that the remaining 30% of IN cell-types, e.g. 5HT3a receptor-
360 expressing neurons, also contribute to the reduced mIPSC frequency observed in *Disc1* LI
361 mice. Next, IPSCs directly evoked by optogenetic stimulation significantly overlapped at short
362 interstimulus intervals; therefore changes in the input resistance due to open channels likely
363 influenced the size of the second signal and hence the PPR measurement. More detailed

364 analysis such as multiple probability-compound binomial analysis or direct analysis of failure
365 rate is necessary to conclude that GABA release probability from PV INs is reduced in *Disc1* LI
366 mice. We observed that PV IN evoked IPSC PPR was significantly increased at the 50 and 100
367 ms interstimulus intervals but not at the 150 ms interval. The time dependence of this effect may
368 suggest a postsynaptic mechanism, such as GABA mediated regulation of PPR (Kirischuk et al.,
369 2002). Alternatively, GABAB presynaptic regulation may play a role in influencing PPR.
370 Interestingly, a reduction in $GABA_B$ receptor expression in PNs has been observed in
371 postmortem brain tissue of individuals with schizophrenia (Mizukami et al., 2002). These
372 caveats considered, we provide multiple lines of evidence that are consistent with elevated E-I
373 balance and abnormal PV IN function in mPFC circuits in *Disc1* LI mice.

374 The coordinated activity between the MD and the PFC is important for working memory,
375 attention, and flexible goal-oriented behavior (Mitchell and Chakraborty, 2013; Parnaudeau et
376 al., 2013; Parnaudeau et al., 2015; Schmitt et al., 2017; Alcaraz et al., 2018), faculties that are
377 impaired in a variety of psychiatric disorders. Meanwhile, studies have found that MD-mPFC
378 synaptic strength is modulated by social interaction, perhaps relevant to negative symptoms of
379 schizophrenia and depression (Northoff and Sibille, 2014; Franklin et al., 2017; Zhou et al.,
380 2017). In relation to DISC1, one study found that a common missense variant of *Disc1* was
381 associated with altered thalamofrontal functional connectivity (Liu et al., 2015). Notably, patients
382 with schizophrenia and bipolar disorder exhibit reduced MD-PFC functional connectivity relative
383 to healthy controls (Welsh et al., 2010; Woodward et al., 2012; Anticevic et al., 2014). An
384 emerging hypothesis posits that local disinhibition of PFC may destabilize the flow of information
385 through the thalamofrontal loop and contribute to cognitive and negative symptoms in
386 schizophrenia and related disorders (Anticevic et al., 2012; Murray and Anticevic, 2017).
387 Structural alterations within thalamofrontal circuits have also been linked to cognitive deficits
388 associated with aging (Hughes et al., 2012) and epilepsy (Pulsipher et al., 2009). However, until
389 recently there was a paucity of data describing how the MD and frontal cortex interact at the

neural circuit level. Recent studies have demonstrated that the MD thalamus recruits feedforward inhibition in the rodent mPFC (Delevich et al., 2015; Miller et al., 2017; Collins et al., 2018; Meda et al., 2019) that is primarily mediated by PV INs (Delevich et al., 2015). Interestingly, chemogenetic excitation of mPFC PV INs has been shown to rescue cognitive deficits induced by chemogenetic inhibition of MD (Ferguson and Gao, 2018b).

Our findings extend data suggesting that MD, via its projections to PV INs, is a key regulator of E-I balance that underpins prefrontal cortex circuit function. We demonstrate that reduced DISC1 expression, a key molecular candidate to study biology relevant to behavioral constructs related to several psychiatric disorders, leads to elevated E-I balance in the MD-mPFC thalamofrontal circuit. Given that few treatment options exist to address the cognitive symptoms of psychiatric disorders, efforts towards understanding the cellular and molecular mechanisms underlying abnormal thalamofrontal functional connectivity may yield therapies that will improve patient outcomes.

References:

Alcaraz F, Fresno V, Marchand AR, Kremer EJ, Coutureau E, Wolff M (2018) Thalamocortical and corticothalamic pathways differentially contribute to goal-directed behaviors in the rat. eLife 7.

Anticevic A, Cole MW, Repovs G, Murray JD, Brumbaugh MS, Winkler AM, Savic A, Krystal JH, Pearlson GD, Glahn DC (2014) Characterizing thalamo-cortical disturbances in schizophrenia and bipolar illness. Cereb Cortex 24:3116-3130.

Anticevic A, Gancsos M, Murray JD, Repovs G, Driesen NR, Ennis DJ, Niciu MJ, Morgan PT, Surti TS, Bloch MH, Ramani R, Smith MA, Wang XJ, Krystal JH, Corlett PR (2012) NMDA receptor function in large-scale anticorrelated neural systems with implications for cognition and schizophrenia. Proc Natl Acad Sci U S A 109:16720-16725.

Antoine MW, Langberg T, Schnepel P, Feldman DE (2019) Increased Excitation-Inhibition Ratio Stabilizes Synapse and Circuit Excitability in Four Autism Mouse Models. Neuron 101:648-661 e644.

Ayhan Y, Abazyan B, Nomura J, Kim R, Ladenheim B, Krasnova IN, Sawa A, Margolis RL, Cadet JL, Mori S, Vogel MW, Ross CA, Pletnikov MV (2011) Differential effects of prenatal and postnatal expressions of mutant human DISC1 on neurobehavioral phenotypes in transgenic mice: evidence for neurodevelopmental origin of major psychiatric disorders. Mol Psychiatry 16:293-306.

Beasley CL, Reynolds GP (1997) Parvalbumin-immunoreactive neurons are reduced in the prefrontal cortex of schizophrenics. Schizophrenia research 24:349-355.

426 Bolkan SS, Stujenske JM, Parnaudeau S, Spellman TJ, Rauffenbart C, Abbas AI, Harris AZ,
427 Gordon JA, Kellendonk C (2017) Thalamic projections sustain prefrontal activity during
428 working memory maintenance. Nature neuroscience 20:987-996.
429 Brandon NJ, Sawa A (2011) Linking neurodevelopmental and synaptic theories of mental illness
430 through DISC1. Nat Rev Neurosci 12:707-722.
431 Burdick KE, Hodgkinson CA, Szeszko PR, Lencz T, Ekholm JM, Kane JM, Goldman D,
432 Malhotra AK (2005) DISC1 and neurocognitive function in schizophrenia. Neuroreport
433 16:1399-1402.
434 Cannon TD, Huttunen MO, Lonnqvist J, Tuulio-Henriksson A, Pirkola T, Glahn D, Finkelstein J,
435 Hietanen M, Kaprio J, Koskenvuo M (2000) The inheritance of neuropsychological
436 dysfunction in twins discordant for schizophrenia. Am J Hum Genet 67:369-382.
437 Cannon TD, Hennah W, van Erp TG, Thompson PM, Lonnqvist J, Huttunen M, Gasperoni T,
438 Tuulio-Henriksson A, Pirkola T, Toga AW, Kaprio J, Mazziotta J, Peltonen L (2005)
439 Association of DISC1/TRAX haplotypes with schizophrenia, reduced prefrontal gray
440 matter, and impaired short- and long-term memory. Arch Gen Psychiatry 62:1205-1213.
441 Cardin JA, Carlen M, Meletis K, Knoblich U, Zhang F, Deisseroth K, Tsai LH, Moore CI (2009)
442 Driving fast-spiking cells induces gamma rhythm and controls sensory responses.
443 Nature 459:663-667.
444 Carless MA, Glahn DC, Johnson MP, Curran JE, Bozaoglu K, Dyer TD, Winkler AM, Cole SA,
445 Almasy L, MacCluer JW, Duggirala R, Moses EK, Goring HH, Blangero J (2011) Impact
446 of DISC1 variation on neuroanatomical and neurocognitive phenotypes. Mol Psychiatry
447 16:1096-1104, 1063.
448 Cho KK, Hoch R, Lee AT, Patel T, Rubenstein JL, Sohal VS (2015) Gamma rhythms link
449 prefrontal interneuron dysfunction with cognitive inflexibility in Dlx5/6(+/-) mice. Neuron
450 85:1332-1343.
451 Chu HY, Ito W, Li J, Morozov A (2012) Target-specific suppression of GABA release from
452 parvalbumin interneurons in the basolateral amygdala by dopamine. J Neurosci
453 32:14815-14820.
454 Clapcote SJ, Lipina TV, Millar JK, Mackie S, Christie S, Ogawa F, Lerch JP, Trimble K,
455 Uchiyama M, Sakuraba Y, Kaneda H, Shiroishi T, Houslay MD, Henkelman RM, Sled
456 JG, Gondo Y, Porteous DJ, Roder JC (2007) Behavioral phenotypes of Disc1 missense
457 mutations in mice. Neuron 54:387-402.
458 Collins DP, Anastasiades PG, Marlin JJ, Carter AG (2018) Reciprocal Circuits Linking the
459 Prefrontal Cortex with Dorsal and Ventral Thalamic Nuclei. Neuron 98:366-379 e364.
460 Delevich K, Tucciarone J, Huang ZJ, Li B (2015) The mediodorsal thalamus drives feedforward
461 inhibition in the anterior cingulate cortex via parvalbumin interneurons. J Neurosci
462 35:5743-5753.
463 Ferguson BR, Gao WJ (2018a) PV Interneurons: Critical Regulators of E/I Balance for
464 Prefrontal Cortex-Dependent Behavior and Psychiatric Disorders. Front Neural Circuits
465 12:37.
466 Ferguson BR, Gao WJ (2018b) Thalamic Control of Cognition and Social Behavior Via
467 Regulation of Gamma-Aminobutyric Acidergic Signaling and Excitation/Inhibition
468 Balance in the Medial Prefrontal Cortex. Biological psychiatry 83:657-669.
469 Franklin TB, Silva BA, Perova Z, Marrone L, Masferrer ME, Zhan Y, Kaplan A, Greetham L,
470 Verrechia V, Halman A, Pagella S, Vyssotski AL, Illarionova A, Grinevich V, Branco T,
471 Gross CT (2017) Prefrontal cortical control of a brainstem social behavior circuit. Nature
472 neuroscience 20:260-270.
473 Fries P (2009) Neuronal gamma-band synchronization as a fundamental process in cortical
474 computation. Annual review of neuroscience 32:209-224.

475 Hashimoto T, Volk DW, Eggan SM, Mirnics K, Pierri JN, Sun Z, Sampson AR, Lewis DA (2003)
476 Gene expression deficits in a subclass of GABA neurons in the prefrontal cortex of
477 subjects with schizophrenia. J Neurosci 23:6315-6326.
478 Hayashi-Takagi A, Takaki M, Graziane N, Seshadri S, Murdoch H, Dunlop AJ, Makino Y,
479 Seshadri AJ, Ishizuka K, Srivastava DP, Xie Z, Baraban JM, Houslay MD, Tomoda T,
480 Brandon NJ, Kamiya A, Yan Z, Penzes P, Sawa A (2010) Disrupted-in-Schizophrenia 1
481 (DISC1) regulates spines of the glutamate synapse via Rac1. Nat Neurosci 13:327-332.
482 Hennah W, Tuulio-Henriksson A, Paunio T, Ekelund J, Varilo T, Partonen T, Cannon TD,
483 Lonnqvist J, Peltonen L (2005) A haplotype within the DISC1 gene is associated with
484 visual memory functions in families with a high density of schizophrenia. Mol Psychiatry
485 10:1097-1103.
486 Hikida T, Jaaro-Peled H, Seshadri S, Oishi K, Hookway C, Kong S, Wu D, Xue R, Andrade M,
487 Tankou S, Mori S, Gallagher M, Ishizuka K, Pletnikov M, Kida S, Sawa A (2007)
488 Dominant-negative DISC1 transgenic mice display schizophrenia-associated
489 phenotypes detected by measures translatable to humans. Proc Natl Acad Sci U S A
490 104:14501-14506.
491 Hippenmeyer S, Vrieseling E, Sigrist M, Portmann T, Laengle C, Ladle DR, Arber S (2005) A
492 developmental switch in the response of DRG neurons to ETS transcription factor
493 signaling. PLoS Biol 3:e159.
494 Holley SM, Wang EA, Cepeda C, Jentsch JD, Ross CA, Pletnikov MV, Levine MS (2013)
495 Frontal cortical synaptic communication is abnormal in Disc1 genetic mouse models of
496 schizophrenia. Schizophr Res 146:264-272.
497 Hughes EJ, Bond J, Svrckova P, Makropoulos A, Ball G, Sharp DJ, Edwards AD, Hajnal JV,
498 Counsell SJ (2012) Regional changes in thalamic shape and volume with increasing
499 age. Neuroimage 63:1134-1142.
500 Ibi D, Nagai T, Koike H, Kitahara Y, Mizoguchi H, Niwa M, Jaaro-Peled H, Nitta A, Yoneda Y,
501 Nabeshima T, Sawa A, Yamada K (2010) Combined effect of neonatal immune
502 activation and mutant DISC1 on phenotypic changes in adulthood. Behav Brain Res
503 206:32-37.
504 Isaacson JS, Scanziani M (2011) How inhibition shapes cortical activity. Neuron 72:231-243.
505 Ishizuka K, Kamiya A, Oh EC, Kanki H, Seshadri S, Robinson JF, Murdoch H, Dunlop AJ, Kubo
506 K, Furukori K, Huang B, Zeledon M, Hayashi-Takagi A, Okano H, Nakajima K, Houslay
507 MD, Katsanis N, Sawa A (2011) DISC1-dependent switch from progenitor proliferation to
508 migration in the developing cortex. Nature 473:92-96.
509 Ishizuka K et al. (2007) Evidence that many of the DISC1 isoforms in C57BL/6J mice are also
510 expressed in 129S6/SvEv mice. Mol Psychiatry 12:897-899.
511 Jaaro-Peled H et al. (2018) The cortico-striatal circuit regulates sensorimotor gating via
512 Disc1/Huntingtin-mediated Bdnf transport. bioRxiv:497446.
513 Kamiya A, Kubo K, Tomoda T, Takaki M, Youn R, Ozeki Y, Sawamura N, Park U, Kudo C,
514 Okawa M, Ross CA, Hatten ME, Nakajima K, Sawa A (2005) A schizophrenia-
515 associated mutation of DISC1 perturbs cerebral cortex development. Nat Cell Biol
516 7:1167-1178.
517 Kehrer C, Maziashvili N, Dugladze T, Gloveli T (2008) Altered Excitatory-Inhibitory Balance in
518 the NMDA-Hypofunction Model of Schizophrenia. Front Mol Neurosci 1:6.
519 Kirischuk S, Clements JD, Grantyn R (2002) Presynaptic and postsynaptic mechanisms
520 underlie paired pulse depression at single GABAergic boutons in rat collicular cultures. J
521 Physiol 543:99-116.
522 Koike H, Arguello PA, Kvajo M, Karayiorgou M, Gogos JA (2006) Disc1 is mutated in the
523 129S6/SvEv strain and modulates working memory in mice. Proc Natl Acad Sci U S A
524 103:3693-3697.

525 Koyanagi Y, Yamamoto K, Oi Y, Koshikawa N, Kobayashi M (2010) Presynaptic interneuron
526 subtype- and age-dependent modulation of GABAergic synaptic transmission by beta-
527 adrenoceptors in rat insular cortex. J Neurophysiol 103:2876-2888.
528 Krystal JH, Anticevic A, Yang GJ, Dragoi G, Driesen NR, Wang XJ, Murray JD (2017) Impaired
529 Tuning of Neural Ensembles and the Pathophysiology of Schizophrenia: A Translational
530 and Computational Neuroscience Perspective. Biol Psychiatry 81:874-885.
531 Kuroda M, Yokofujita J, Murakami K (1998) An ultrastructural study of the neural circuit between
532 the prefrontal cortex and the mediodorsal nucleus of the thalamus. Progress in
533 neurobiology 54:417-458.
534 Kvajo M, McKellar H, Arguello PA, Drew LJ, Moore H, MacDermott AB, Karayiorgou M, Gogos
535 JA (2008) A mutation in mouse Disc1 that models a schizophrenia risk allele leads to
536 specific alterations in neuronal architecture and cognition. Proc Natl Acad Sci U S A
537 105:7076-7081.
538 Lee FH, Zai CC, Cordes SP, Roder JC, Wong AH (2013) Abnormal interneuron development in
539 disrupted-in-schizophrenia-1 L100P mutant mice. Mol Brain 6:20.
540 Lesh TA, Niendam TA, Minzenberg MJ, Carter CS (2011) Cognitive control deficits in
541 schizophrenia: mechanisms and meaning. Neuropsychopharmacology 36:316-338.
542 Lewis DA, Curley AA, Glausier JR, Volk DW (2012) Cortical parvalbumin interneurons and
543 cognitive dysfunction in schizophrenia. Trends Neurosci 35:57-67.
544 Li H, Penzo MA, Taniguchi H, Kopec CD, Huang ZJ, Li B (2013) Experience-dependent
545 modification of a central amygdala fear circuit. Nat Neurosci 16:332-339.
546 Li W, Zhou Y, Jentsch JD, Brown RA, Tian X, Ehninger D, Hennah W, Peltonen L, Lonnqvist J,
547 Huttunen MO, Kaprio J, Trachtenberg JT, Silva AJ, Cannon TD (2007) Specific
548 developmental disruption of disrupted-in-schizophrenia-1 function results in
549 schizophrenia-related phenotypes in mice. Proc Natl Acad Sci U S A 104:18280-18285.
550 Lipina TV, Niwa M, Jaaro-Peled H, Fletcher PJ, Seeman P, Sawa A, Roder JC (2010)
551 Enhanced dopamine function in DISC1-L100P mutant mice: implications for
552 schizophrenia. Genes Brain Behav 9:777-789.
553 Lisman J (2012) Excitation, inhibition, local oscillations, or large-scale loops: what causes the
554 symptoms of schizophrenia? Curr Opin Neurobiol 22:537-544.
555 Liu B, Fan L, Cui Y, Zhang X, Hou B, Li Y, Qin W, Wang D, Yu C, Jiang T (2015) DISC1
556 Ser704Cys impacts thalamic-prefrontal connectivity. Brain Struct Funct 220:91-100.
557 Liu YL, Fann CS, Liu CM, Chen WJ, Wu JY, Hung SI, Chen CH, Jou YS, Liu SK, Hwang TJ,
558 Hsieh MH, Ouyang WC, Chan HY, Chen JJ, Yang WC, Lin CY, Lee SF, Hwu HG (2006)
559 A single nucleotide polymorphism fine mapping study of chromosome 1q42.1 reveals the
560 vulnerability genes for schizophrenia, GNPAT and DISC1: Association with impairment
561 of sustained attention. Biol Psychiatry 60:554-562.
562 Ma Y, Hu H, Agmon A (2012) Short-term plasticity of unitary inhibitory-to-inhibitory synapses
563 depends on the presynaptic interneuron subtype. J Neurosci 32:983-988.
564 Madisen L, Zwingman TA, Sunkin SM, Oh SW, Zariwala HA, Gu H, Ng LL, Palmiter RD,
565 Hawrylycz MJ, Jones AR, Lein ES, Zeng H (2010) A robust and high-throughput Cre
566 reporting and characterization system for the whole mouse brain. Nat Neurosci 13:133-
567 140.
568 Maher BJ, LoTurco JJ (2012) Disrupted-in-schizophrenia (DISC1) functions presynaptically at
569 glutamatergic synapses. PLoS One 7:e34053.
570 Mao Y, Ge X, Frank CL, Madison JM, Koehler AN, Doud MK, Tassa C, Berry EM, Soda T,
571 Singh KK, Biechele T, Petryshen TL, Moon RT, Haggarty SJ, Tsai LH (2009) Disrupted
572 in schizophrenia 1 regulates neuronal progenitor proliferation via modulation of
573 GSK3beta/beta-catenin signaling. Cell 136:1017-1031.
574 Marin O (2012) Interneuron dysfunction in psychiatric disorders. Nat Rev Neurosci 13:107-120.

575 Meda KS, Patel T, Braz JM, Malik R, Turner ML, Seifikar H, Basbaum AI, Sohal VS (2019)
576 Microcircuit Mechanisms through which Mediodorsal Thalamic Input to Anterior
577 Cingulate Cortex Exacerbates Pain-Related Aversion. Neuron 102:944-959 e943.
578 Meyer KD, Morris JA (2008) Immunohistochemical analysis of Disc1 expression in the
579 developing and adult hippocampus. Gene Expr Patterns 8:494-501.
580 Millar JK, Wilson-Annan JC, Anderson S, Christie S, Taylor MS, Semple CA, Devon RS, St Clair
581 DM, Muir WJ, Blackwood DH, Porteous DJ (2000) Disruption of two novel genes by a
582 translocation co-segregating with schizophrenia. Hum Mol Genet 9:1415-1423.
583 Miller OH, Bruns A, Ben Ammar I, Mueggler T, Hall BJ (2017) Synaptic Regulation of a
584 Thalamocortical Circuit Controls Depression-Related Behavior. Cell Rep 20:1867-1880.
585 Mitchell AS, Chakraborty S (2013) What does the mediodorsal thalamus do? Front Syst
586 Neurosci 7:37.
587 Mittmann W, Koch U, Hausser M (2005) Feed-forward inhibition shapes the spike output of
588 cerebellar Purkinje cells. The Journal of physiology 563:369-378.
589 Mizukami K, Ishikawa M, Hidaka S, Iwakiri M, Sasaki M, Iritani S (2002) Immunohistochemical
590 localization of GABAB receptor in the entorhinal cortex and inferior temporal cortex of
591 schizophrenic brain. Prog Neuropsychopharmacol Biol Psychiatry 26:393-396.
592 Murray AJ, Woloszynowska-Fraser MU, Ansel-Bollepalli L, Cole KL, Foggetti A, Crouch B,
593 Riedel G, Wulff P (2015) Parvalbumin-positive interneurons of the prefrontal cortex
594 support working memory and cognitive flexibility. Sci Rep 5:16778.
595 Murray JD, Anticevic A (2017) Toward understanding thalamocortical dysfunction in
596 schizophrenia through computational models of neural circuit dynamics. Schizophr Res
597 180:70-77.
598 Myles-Worsley M, Park S (2002) Spatial working memory deficits in schizophrenia patients and
599 their first degree relatives from Palau, Micronesia. Am J Med Genet 114:609-615.
600 Nicodemus KK, Elvevag B, Foltz PW, Rosenstein M, Diaz-Asper C, Weinberger DR (2014)
601 Category fluency, latent semantic analysis and schizophrenia: a candidate gene
602 approach. Cortex 55:182-191.
603 Niwa M, Cash-Padgett T, Kubo KI, Saito A, Ishii K, Sumitomo A, Taniguchi Y, Ishizuka K, Jaaro-
604 Peled H, Tomoda T, Nakajima K, Sawa A, Kamiya A (2016) DISC1 a key molecular lead
605 in psychiatry and neurodevelopment: No-More Disrupted-in-Schizophrenia 1. Mol
606 Psychiatry 21:1488-1489.
607 Niwa M, Kamiya A, Murai R, Kubo K, Gruber AJ, Tomita K, Lu L, Tomisato S, Jaaro-Peled H,
608 Seshadri S, Hiyama H, Huang B, Kohda K, Noda Y, O'Donnell P, Nakajima K, Sawa A,
609 Nabeshima T (2010) Knockdown of DISC1 by in utero gene transfer disturbs postnatal
610 dopaminergic maturation in the frontal cortex and leads to adult behavioral deficits.
611 Neuron 65:480-489.
612 Northoff G, Sibille E (2014) Why are cortical GABA neurons relevant to internal focus in
613 depression? A cross-level model linking cellular, biochemical and neural network
614 findings. Molecular psychiatry 19:966-977.
615 Palo OM, Antila M, Silander K, Hennah W, Kilpinen H, Soronen P, Tuulio-Henriksson A,
616 Kieseppa T, Partonen T, Lonnqvist J, Peltonen L, Paunio T (2007) Association of distinct
617 allelic haplotypes of DISC1 with psychotic and bipolar spectrum disorders and with
618 underlying cognitive impairments. Hum Mol Genet 16:2517-2528.
619 Parnaudeau S, Bolkan SS, Kellendonk C (2017) The Mediodorsal Thalamus: An Essential
620 Partner of the Prefrontal Cortex for Cognition. Biological psychiatry.
621 Parnaudeau S, Taylor K, Bolkan SS, Ward RD, Balsam PD, Kellendonk C (2015) Mediodorsal
622 thalamus hypofunction impairs flexible goal-directed behavior. Biol Psychiatry 77:445-
623 453.

624 Parnaudeau S, O'Neill PK, Bolkan SS, Ward RD, Abbas AI, Roth BL, Balsam PD, Gordon JA,
625 Kellendonk C (2013) Inhibition of mediodorsal thalamus disrupts thalamofrontal
626 connectivity and cognition. Neuron 77:1151-1162.
627 Pulsipher DT, Seidenberg M, Guidotti L, Tuchscherer VN, Morton J, Sheth RD, Hermann B
628 (2009) Thalamofrontal circuitry and executive dysfunction in recent-onset juvenile
629 myoclonic epilepsy. Epilepsia 50:1210-1219.
630 Rikhye RV, Gilra A, Halassa MM (2018) Thalamic regulation of switching between cortical
631 representations enables cognitive flexibility. Nat Neurosci 21:1753-1763.
632 Rudy B, Fishell G, Lee S, Hjerling-Leffler J (2011) Three groups of interneurons account for
633 nearly 100% of neocortical GABAergic neurons. Dev Neurobiol 71:45-61.
634 Sauer JF, Struber M, Bartos M (2015) Impaired fast-spiking interneuron function in a genetic
635 mouse model of depression. Elife 4.
636 Schizophrenia Working Group of the Psychiatric Genomics C (2014) Biological insights from
637 108 schizophrenia-associated genetic loci. Nature 511:421-427.
638 Schmitt LI, Wimmer RD, Nakajima M, Happ M, Mofakham S, Halassa MM (2017) Thalamic
639 amplification of cortical connectivity sustains attentional control. Nature 545:219-223.
640 Schurov IL, Handford EJ, Brandon NJ, Whiting PJ (2004) Expression of disrupted in
641 schizophrenia 1 (DISC1) protein in the adult and developing mouse brain indicates its
642 role in neurodevelopment. Mol Psychiatry 9:1100-1110.
643 Schwabe K, Koch M (2004) Role of the medial prefrontal cortex in N-methyl-D-aspartate
644 receptor antagonist induced sensorimotor gating deficit in rats. Neurosci Lett 355:5-8.
645 Seshadri S, Faust T, Ishizuka K, Delevich K, Chung Y, Kim SH, Cowles M, Niwa M, Jaaro-Peled
646 H, Tomoda T, Lai C, Anton ES, Li B, Sawa A (2015) Interneuronal DISC1 regulates
647 NRG1-ErbB4 signalling and excitatory-inhibitory synapse formation in the mature cortex.
648 Nat Commun 6:10118.
649 Shahani N, Seshadri S, Jaaro-Peled H, Ishizuka K, Hirota-Tsuyada Y, Wang Q, Koga M, Sedlak
650 TW, Korth C, Brandon NJ, Kamiya A, Subramaniam S, Tomoda T, Sawa A (2015)
651 DISC1 regulates trafficking and processing of APP and Abeta generation. Mol Psychiatry
652 20:874-879.
653 Shen S, Lang B, Nakamoto C, Zhang F, Pu J, Kuan SL, Chatzi C, He S, Mackie I, Brandon NJ,
654 Marquis KL, Day M, Hurko O, McCaig CD, Riedel G, St Clair D (2008) Schizophrenia-
655 related neural and behavioral phenotypes in transgenic mice expressing truncated
656 Disc1. J Neurosci 28:10893-10904.
657 Snitz BE, Macdonald AW, 3rd, Carter CS (2006) Cognitive deficits in unaffected first-degree
658 relatives of schizophrenia patients: a meta-analytic review of putative endophenotypes.
659 Schizophr Bull 32:179-194.
660 Sohal VS, Zhang F, Yizhar O, Deisseroth K (2009) Parvalbumin neurons and gamma rhythms
661 enhance cortical circuit performance. Nature 459:698-702.
662 Steinecke A, Gampe C, Valkova C, Kaether C, Bolz J (2012) Disrupted-in-Schizophrenia 1
663 (DISC1) is necessary for the correct migration of cortical interneurons. J Neurosci
664 32:738-745.
665 Swerdlow NR, Geyer MA, Braff DL (2001) Neural circuit regulation of prepulse inhibition of
666 startle in the rat: current knowledge and future challenges. Psychopharmacology (Berl)
667 156:194-215.
668 Taniguchi H, He M, Wu P, Kim S, Paik R, Sugino K, Kvitsiani D, Fu Y, Lu J, Lin Y, Miyoshi G,
669 Shima Y, Fishell G, Nelson SB, Huang ZJ (2011) A resource of Cre driver lines for
670 genetic targeting of GABAergic neurons in cerebral cortex. Neuron 71:995-1013.
671 Wang Q et al. (2011) The psychiatric disease risk factors DISC1 and TNIK interact to regulate
672 synapse composition and function. Mol Psychiatry 16:1006-1023.

673 Wei J, Graziane NM, Gu Z, Yan Z (2015) DISC1 Protein Regulates gamma-Aminobutyric Acid,
674 Type A (GABAA) Receptor Trafficking and Inhibitory Synaptic Transmission in Cortical
675 Neurons. J Biol Chem 290:27680-27687.
676 Welsh RC, Chen AC, Taylor SF (2010) Low-frequency BOLD fluctuations demonstrate altered
677 thalamocortical connectivity in schizophrenia. Schizophr Bull 36:713-722.
678 Woodward ND, Karbasforoushan H, Heckers S (2012) Thalamocortical dysconnectivity in
679 schizophrenia. Am J Psychiatry 169:1092-1099.
680 Yizhar O, Fenno LE, Prigge M, Schneider F, Davidson TJ, O'Shea DJ, Sohal VS, Goshen I,
681 Finkelstein J, Paz JT, Stehfest K, Fudim R, Ramakrishnan C, Huguenard JR, Hegemann
682 P, Deisseroth K (2011) Neocortical excitation/inhibition balance in information
683 processing and social dysfunction. Nature 477:171-178.
684 Zhang F, Wang LP, Boyden ES, Deisseroth K (2006) Channelrhodopsin-2 and optical control of
685 excitable cells. Nat Methods 3:785-792.
686 Zhang F, Wang LP, Brauner M, Liewald JF, Kay K, Watzke N, Wood PG, Bamberg E, Nagel G,
687 Gottschalk A, Deisseroth K (2007) Multimodal fast optical interrogation of neural
688 circuitry. Nature 446:633-639.
689 Zhou T, Zhu H, Fan Z, Wang F, Chen Y, Liang H, Yang Z, Zhang L, Lin L, Zhan Y, Wang Z, Hu
690 H (2017) History of winning remodels thalamo-PFC circuit to reinforce social dominance.
691 Science 357:162-168.
692

693 **Figures legends:**

694 **Figure 1. Reduced inhibitory synaptic transmission onto L2/3 pyramidal neurons in the**
695 **mPFC of adult and juvenile *Disc1* LI mice.** (A) Recording configuration and sample mIPSC
696 traces recorded from L2/3 PNs in the mPFC of WT (upper) and *Disc1* LI (lower) mice at ~P70.
697 (B) mIPSC amplitude (WT, n = 27 cells; *Disc1* LI, n = 29 cells). (C) mIPSC frequency (WT, n =
698 27 cells; *Disc1* LI, n = 29 cells; $^{**}P < 0.01$, Mann-Whitney U test). (D) Recording configuration
699 and sample mEPSC traces recorded from L2/3 PNs in the mPFC of WT (upper) and *Disc1* LI
700 (lower) mice at ~P70. (E) mEPSC amplitude (WT, n = 23 cells; *Disc1* LI, n = 20 cells). (F)
701 mEPSC frequency (WT, n = 23 cells; *Disc1* LI, n = 20 cells). (G) Recording configuration and
702 sample mIPSC traces recorded from L2/3 PNs in the mPFC of WT (upper) and *Disc1* LI (lower)
703 mice at ~P15. (H) mIPSC amplitude (WT, n = 44 cells; *Disc1* LI, n = 26 cells; $P = 0.12$, *t* test)
704 and (I) frequency (WT, n = 44 cells; *Disc1* LI, n = 26 cells; $^{*}P < 0.05$, Mann-Whitney U test). All
705 scale bars represent 20 pA, 500 ms. Bar graphs indicate median ± interquartile range (B, C, F,
706 I) or mean ± s.e.m. (E, H), as appropriate.
707
708 **Figure 2. Impaired presynaptic function of PV but not SOM INs in the mPFC of *Disc1* LI**
709 **mice.** (A) A schematic of the experimental configuration. (B) Sample traces of PV IN-mediated
710 IPSCs recorded from WT (left panel) or *Disc1* LI (right panel) mice. Paired light pulses (1 ms
711 duration; blue bars) were delivered at an interval of 50 ms (top), 100 ms (middle) or 150 ms
712 (bottom). (C) Quantification of PPR for each genotype (WT, n = 13 cells; *Disc1* LI, n = 10 cells).
713 $^{*}P < 0.05$, $^{***}P < 0.001$, two-way repeated measures ANOVA followed by Sidak's test. (D) A
714 schematic of the experimental configuration. (E) Sample traces of SOM IN-mediated IPSCs
715 recorded from WT (left panel) or *Disc1* LI (right panel) mice. Paired light pulses (1 ms duration;
716 blue bars) were delivered at an interval of 50 ms (top), 100 ms (middle) or 150 ms (bottom). (F)
717 Quantification of PPR for each genotype (WT, n = 15 cells, *Disc1* LI, n = 12 cells). (G) Sample
718 IPSC traces evoked by optogenetic stimulation of PV or SOM INs. Colored lines indicate

719 exponential fits to the decays of the IPSCs. (H) Quantification of IPSC decay tau. ****P <
720 0.0001, *t* test. Data in C, F, and H are presented as mean ± s.e.m.
721
722 **Figure 3. Reduced feedforward inhibition in the MD–mPFC circuit in *Disc1* LI mice.** (A &
723 B) Schematics of the experimental configuration. The right panel of (A) is an image of a brain
724 section from a mouse used in electrophysiological recording, showing the MD infected with
725 AAV-CAG-ChR2-YFP. (C) Representative traces of EPSC (recorded at –60 mV) and IPSC
726 (recorded at 0 mV) from L3 PNs. (D) To estimate the relative recruitment of disynaptic FFI
727 versus monosynaptic excitation, we divided peak IPSC (I^{peak}) by the sum of peak IPSC and
728 peak EPSC (I^{peak} + E^{peak}). WT, N = 14 mice, *Disc1* LI, N = 11 mice; ***P < 0.001, *t* test. (E)
729 Same as in (D), except that the cumulative probability distributions of the values for individual
730 neurons are shown. WT, n = 40 cells, *Disc1* LI, n = 30 cells; **P < 0.01, Kolmogorov-Smirnov
731 test. (F) Scatter plot showing the peak amplitudes of IPSC and EPSC for individual neurons.
732 Each circle represents one neuron (WT, n = 30 cells; *Disc1* LI, n = 40 cells). Dashed lines are
733 linear regression lines for neurons in WT mice and *Disc1* LI mice. The slopes of the regression
734 lines significantly differed at the 0.95 confidence level (*P < 0.05). (G) Sample traces of IPSC
735 (recorded at 0 mV) and EPSC (recorded at –60 mV) recorded from L2/3 PNs in response to
736 light-stimulation (blue bars) of MD axons. The latency to onset was measured from the time the
737 light stimulus was triggered to the 10% EPSC (blue arrow) or IPSC (red arrow) rise time. Note
738 that IPSC rise time was calculated from the peak of the inward current recorded at 0 mV. (H)
739 Cumulative probability distributions for EPSC latency to onset (left) and IPSC latency to onset
740 (right) (EPSC, WT, n = 40 cells, *Disc1* LI, n = 30 cells, P = 0.40; IPSC, WT, n = 40 cells, *Disc1*
741 LI, n = 30 cells, P = 0.56; Kolmogorov-Smirnov test). (I) Quantification of IPSC–EPSC lag,
742 calculated as the difference in the latency to onset between the IPSC and the EPSC of each
743 neuron (see also (G) (WT, n = 40 cells, *Disc1* LI, n = 30 cells; P > 0.05, *t* test). (J) Quantification
744 of the 10-90% EPSC rise time and decay tau (K) (WT, n = 40 cells, *Disc1* LI, n = 30 cells; P >

745 0.05, Mann-Whitney U test). (L) Quantification of the 10-90% IPSC rise time and decay tau (M)
746 (WT, n = 40 cells, *Disc1* LI, n = 28 cells; $P > 0.05$, t test). Data are presented as median ±
747 interquartile range (J,K) or mean ± s.e.m. (D, L, M).
748
749 **Figure 4. mEPSCs and intrinsic properties of PV INs are not altered in *Disc1* LI mice.** (A)
750 Recording configuration and sample mEPSC traces recorded from PV INs in WT (upper) and
751 *Disc1* LI mice (lower). (B) Mean mEPSC amplitude (left) and median frequency (right) (n= 20,
752 23 cells/genotype; N= 4 mice/genotype). (C) Sample traces from whole cell current clamp
753 recording of L2/3 PV IN in WT (left) and *Disc1* LI mouse in response to current injections. (D)
754 Input-output curve showing average firing rate of PV INs in response to current injection in WT
755 vs. *Disc1* LI. (E) Resting membrane potential (F) Input resistance (G) Current threshold required
756 to elicit spiking (H) Maximum firing rate. Data in D, E, H shown as mean ± s.e.m. Data in F, G
757 shown as median ± interquartile range.
758
759 **Figure 5. Impaired presynaptic function of PV INs underlies the deficit of FFI in *Disc1* LI**
760 **mice.** (A) Left: a schematic of the experimental configuration. Right: a schematic of the
761 recording configuration in the mPFC acute slices. A Tdtomato^{+} PV IN (red) and an adjacent PN
762 (gray) in L3 of the mPFC were recorded simultaneously or sequentially. EPSCs onto these
763 neurons were evoked by optogenetic stimulation (0.5 ms light pulses; blue bars) of MD axons.
764 (B) Sample EPSC traces recorded from PV IN and PN pairs are superimposed and color-coded.
765 (C) Quantification of the EPSC peak amplitude. n.s., not significant ($P = 1.0$); $^{**}P < 0.01$;
766 Wilcoxon matched-pairs signed ranks test. (D) Sample traces of FFI currents recorded from L3
767 PNs in response to optogenetic stimulation of MD axons. (E) Quantification of PPR of the MD-
768 driven FFI onto L3 PNs. $^{***}P < 0.001$, Mann-Whitney U test. (F) The mean amplitude of the first
769 IPSC was consistent between genotypes. Data in E presented as median ± interquartile range
770 data in F presented as mean ± s.e.m. (G) FFI PPR plotted against $(I^{peak})/(I^{peak} + E^{peak})$ (as seen

in Fig. 3D) within cells shows that for *Disc1* LI mice but not WT mice, FFI PPR inversely correlated with $(I^{peak})/(I^{peak} + E^{peak})$, suggesting that synapses with high FFI PPR also exhibit higher E/I ratio **P <0.01.

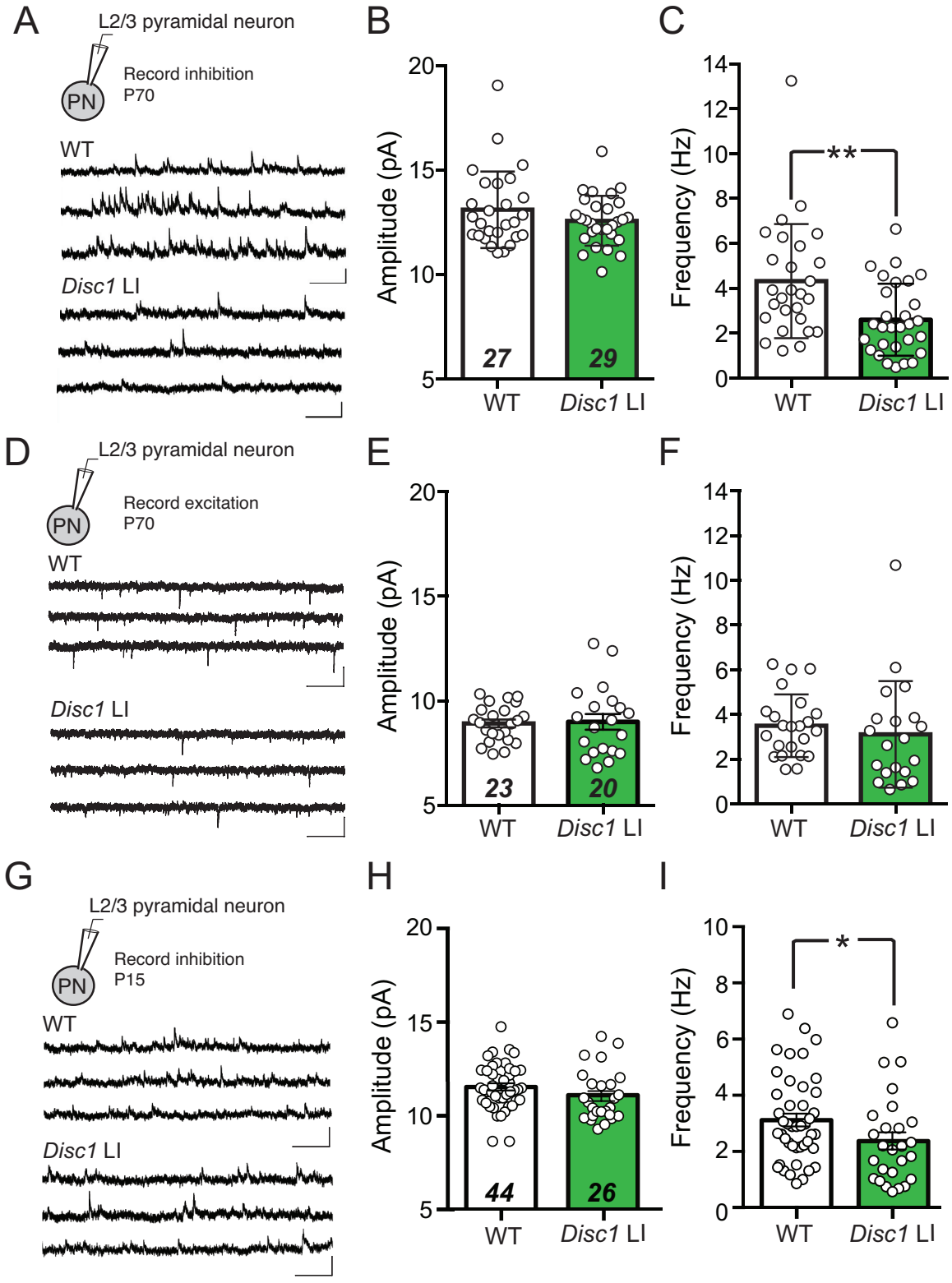

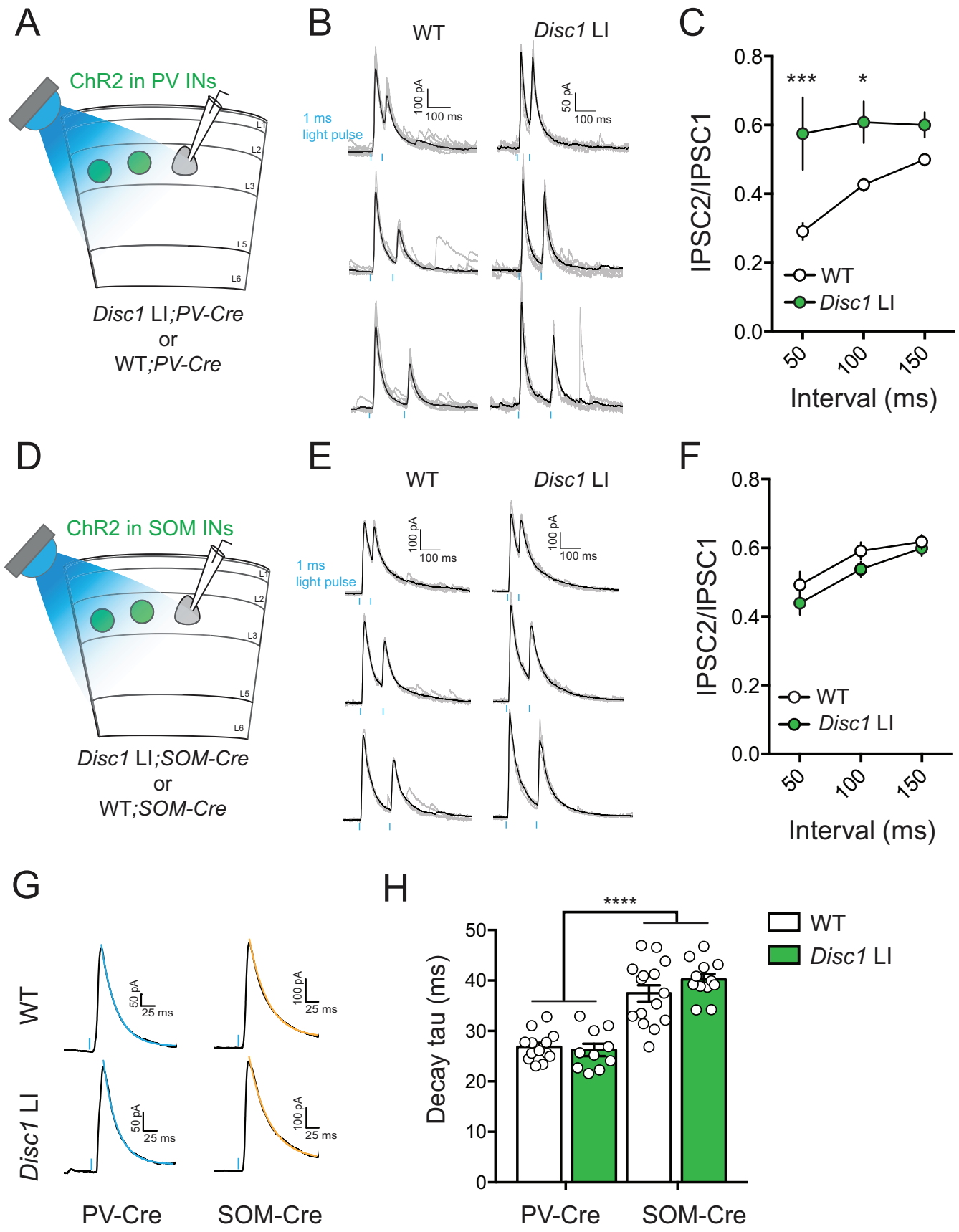

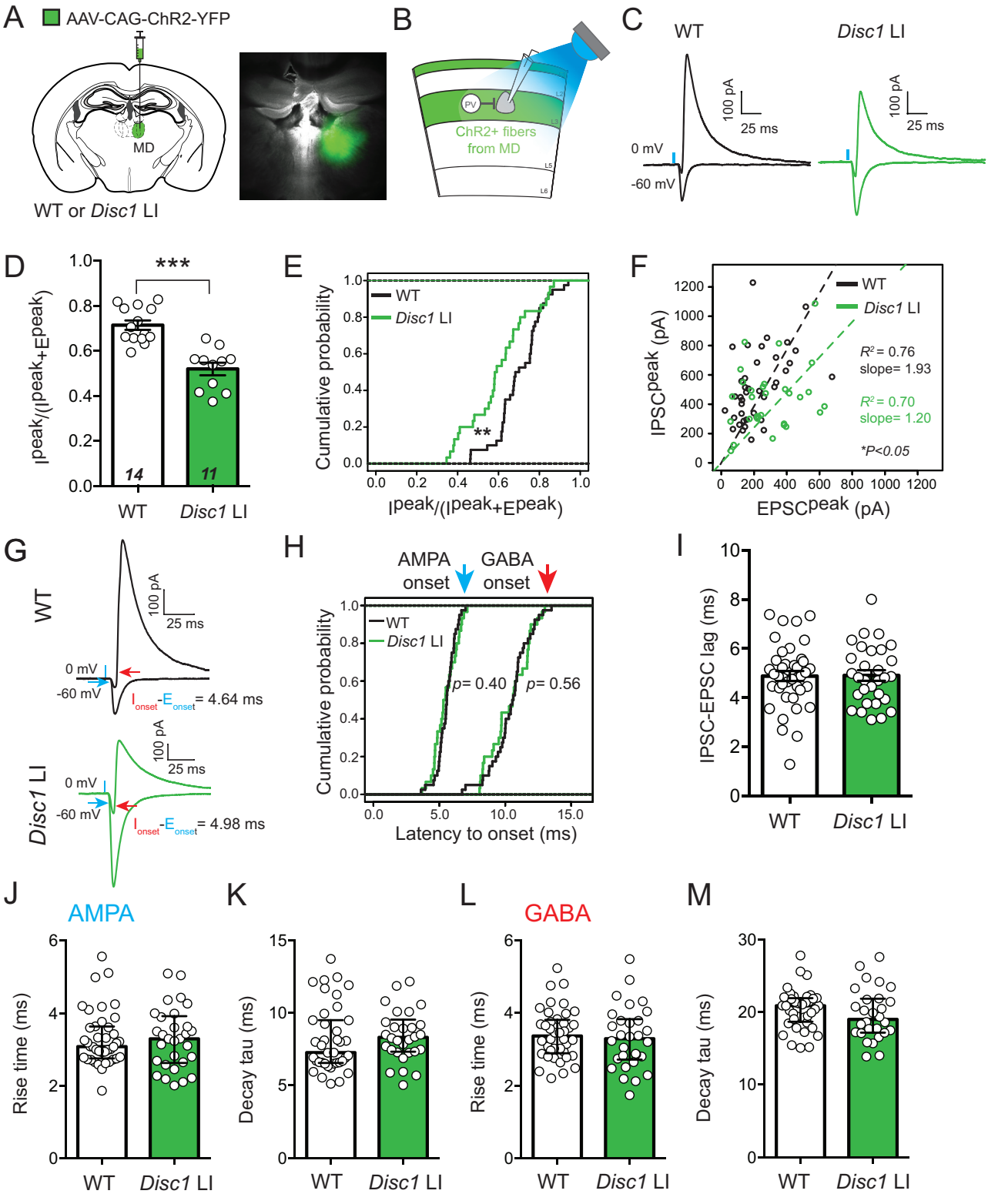

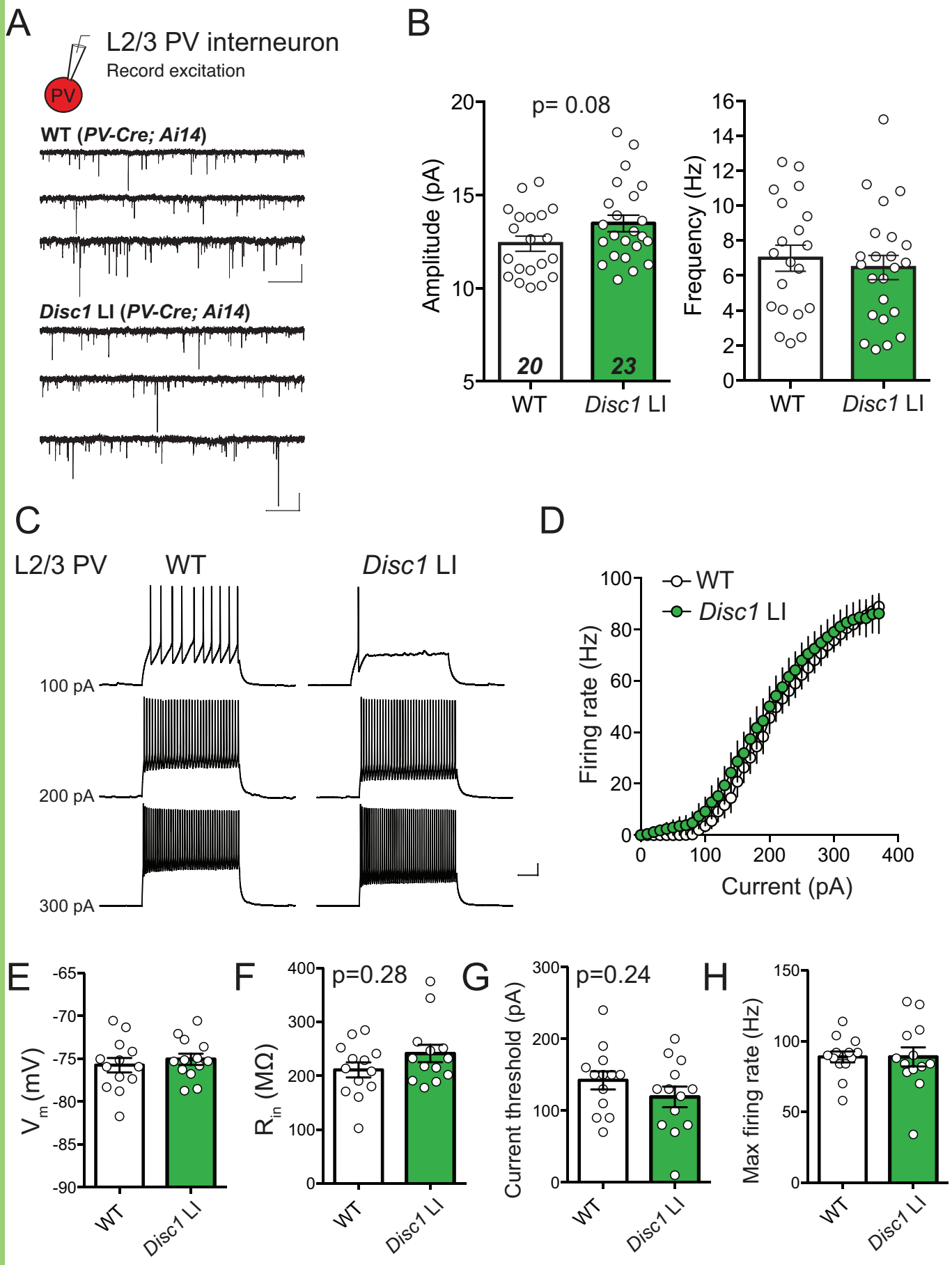

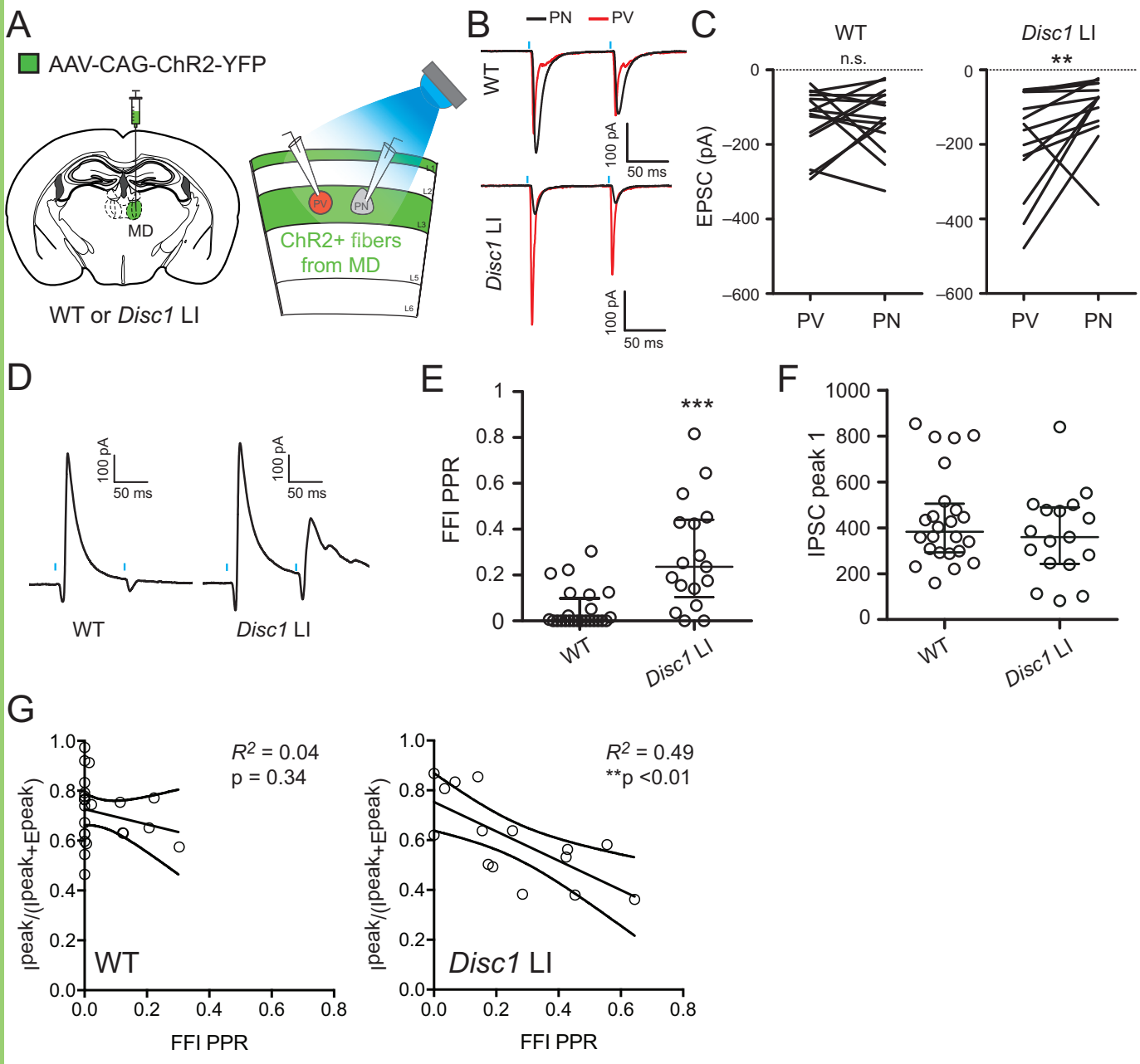

Table 1 — Statistical tests and significance threshold used for each comparison.

Data structure	Statistical test, post hoc	Significance threshold
[a]Non-normal distribution	Two-tailed Mann Whitney U test	P<0.05
[b]Non-normal distribution	Two-tailed Mann Whitney U test	P<0.05
[c]Non-normal distribution	Two-tailed Mann Whitney U test	P<0.05
[d]Normal distribution	Two-tailed unpaired t test	P<0.05
[e]Normal distribution	Two-tailed unpaired t test	P<0.05
[f]Non-normal distribution	Two-tailed Mann Whitney U test	P<0.05
[g]Normal distribution	Two-way repeated measures ANOVA with post hoc Sidak's test	P<0.05
[h]Normal distribution	Two-way repeated measures ANOVA with post hoc Sidak's test	P<0.05
[i]Normal distribution	Two-way ANOVA	P<0.05
[j]Normal distribution	Two-tailed unpaired t test	P<0.05
[k]Normal distribution	Two-tailed unpaired t test	P<0.05
[l]Normal distribution	Two-tailed unpaired t test	P<0.05
[m]Normal distribution	Two-tailed unpaired t test	P<0.05
[n]Normal distribution	Two-tailed unpaired t test	P<0.05
[o]Normal distribution	Two-tailed unpaired t test	P<0.05
[p]Non-normal distribution	Wilcoxon matched-pairs signed ranks test	P<0.05
[q]Non-normal distribution	Wilcoxon matched-pairs signed ranks test	P<0.05
[r]Non-normal distribution	Two-tailed Mann Whitney U test	P<0.05
[s]Non-normal distribution	Two-tailed Mann Whitney U test	P<0.05